Optical and Quantum Electronics (2022) 54:810
https://doi.org/10.1007/s11082-022-04170-0

Calculation of intersubband absorption in ZnO/ZnMgO asymmetric double quantum wells

Aleksandar Atić[1,2,3] · Nikola Vuković[1,3] · Jelena Radovanović[1,3]

Received: 19 July 2022 / Accepted: 4 September 2022 / Published online: 30 September 2022

Abstract
ZnO based heterostructures have recently received increased research attention, related to the development of room temperature THz/MiR semiconductor devices. The potential for these applications stems from the combination of wide direct bandgap and high exciton binding energy. In this work, we focus on the intersubband transition between bound states in the conduction band, and apply self-consistent numerical modelling to a system of Schrödinger–Poisson equations to evaluate the electronics structure of coupled semiconductor quantum wells. We subsequently analyse the fractional optical absorption at room temperature, as it varies with layers' thicknesses, doping density and external electric field magnitude.

Keywords Optical devices · Terahertz · Zinc oxide · Absorption

1 Introduction

The study of optical transitions between bound states in the conduction band of semiconductor-based quantum well structures is crucial for the design of devices such as resonant tunnelling diodes, infrared detectors, quantum cascade lasers, etc. (Faist 2013; Isić et al. 2007; Jirauschek and Kubis 2014; Vukovic et al. 2020). By using advanced methods for precise electronic structure modelling, combined with sophisticated optimization tools (Radovanović et al. 2021, 2007, 2006), the energy of these transitions can be adjusted to provide a wide range of detection/emission values attractive for applications (Vukovic et al. 2016a, 2016b, 2017), both in the near and middle infrared (Dubajić et al. 2018; Gajić et al.

This article is part of the Topical Collection on Photonics: Current Challenges and Emerging Applications, Guest edited by Jelena Radovanovic, Dragan Indjin, Maja Nesic, Nikola Vukovic and Milena Milosevic.

✉ Aleksandar Atić
atic@vin.bg.ac.rs

[1] School of Electrical Engineering, University of Belgrade, Belgrade, Serbia

[2] Vinča Institute of Nuclear Sciences, National Institute of Republic of Serbia, University of Belgrade, Belgrade, Serbia

[3] Centre for Light-Based Research and Technologies COHERENCE, Belgrade, Serbia

2021; Vukovic et al. 2014), and in the terahertz range (Bellotti and Paiella 2010). Quantum cascade detectors consisting of identical periods of QW structures have attracted much attention due to their potential applications for near- or mid-infrared spectroscopy, astronomical observations, commercial and military technology (He et al. 2017; Liu 2022; Liu et al. 2018; Tkach et al. 2015). The terahertz region spans from 1 to 10 THz, corresponding to wavelengths between 300 μm and 30 μm, and is often associated with the term "terahertz gap", implying the shortage of devices for emission/detection of radiation in this region that are commercially available (Köhler et al. 2002). The most common semiconductor for the realization of THz QCLs, GaAs, yields a well-known problem of insufficiently high operating temperature due to large non-radiative losses (Bellotti and Paiella 2010; Lee and Wanke 2007). In order to overcome this obstacle and expand the range of operating conditions of existing devices, assessment of new combinations of semiconductor materials, together with meticulous modelling of intersubband transition related properties, is of utmost importance (Vuković et al. 2022).Wide energy gap semiconductors represent a new field of research that includes the synthesis of different materials and their combinations, testing their physical properties, realization of devices and their subsequent applications in electronics, optoelectronics, and quantum electronics (Higashiwaki et al. 2021). Compared to silicon and III-V compounds, the development of these materials and corresponding devices is at a very early stage. Interest in wide bandgap semiconductors was previously directed at II-VI materials and AlGaN/GaN systems (Gmachl et al. 2000a, 2000b; Radovanovic et al. 2003; Suzuki and Iizuka 1997). However, II-VI compounds are based on complex quaternary alloys, while the standard c-GaN has strong internal polarization fields which hampers the design possibilities and synthesis of such structures (Shirazi-HD et al. 2016). In non-polar GaN, there are no internal fields (Radosavljević et al. 2015, 2014), but the growth is very demanding, and the size of the wafer is limited, which is unfavourable for the realization of devices. It is important to note that experimental realizations in the field of new materials are traditionally preceded by theoretical estimations. The role of such efforts is to predict the properties and to assess the potential of materials and their heterostructures, starting from the calculations of the electronic structure, the influence of dopants and the like.

In this contribution we numerically investigate a structure based on asymmetric quantum wells, realized from oxide materials with a large energy gap i.e., ZnO/ZnMgO heterostructures. These structures are promising candidates for the realization of terahertz emitters for room temperature operation, owing to favourable parameter values and higher resonant energy of longitudinal optical phonons compared to GaAs. Zinc oxide (ZnO) has a direct and wide energy gap (3.37 eV) and higher LO phonon energy (0.72 meV) (Meng et al. 2019), which makes it suitable for the development of new emitters and detectors in the terahertz region of the spectrum (Lee and Wanke 2007; Mang et al. 1995). ZnMgO is an excellent material for electron transporting because its bandgap can be continually tuned from about 3.3 eV to 7.8 eV (Cao et al. 2021), and its lattice constant is close to that of ZnO (Chen et al. 2021; Li et al. 2010). ZnO/ZnMgO devices can lase in the UV range (0.370–0.380 μm) and simulations show that ZnO semiconductors can be used as an alternative for GaN material system (Kaminska et al. 2016). Furthermore, a quantum cascade laser for the THz range, realized from the semiconductor alloys of this material, shows promise of running at room temperature (Sirkeli and Hartnagel 2019). This type of laser utilizes multiple quantum well (MQW) structures for the active region. While MQW structures have been grown on various substrates that include sapphire, GaN, Si, etc. (Fujita et al. 2006; Gruber et al. 2004; Park and Ahn 2005; Riane et al. 2017; Zhang et al. 2007), achievement of high-quality ZnO/ZnMgO MQW structures has been limited by the use of

lattice-mismatched substrates (Zhu et al. 2007). Intersubband transitions have only recently been researched and observed in ZnO/ZnMgO structures (Dakhlaoui and Nefzi 2018; He et al. 2017; Meng et al. 2019; Ohtani et al. 2009; Solovyev et al. 2015; Solovyev and Kukushkin 2019; Sun and Zhang 2008; Zhao et al. 2014; Zhu et al. 2013). Liu has theoretically analysed intersubband optical absorptions in triple ZnO/ZnMgO quantum wells at 70 K temperature with barrier doping (Liu 2022).

Here a Schrödinger–Poisson (SP) system of equations is solved self consistently (Datta 2005) for an asymmetric double quantum well (ADQW) that consists of a wide uniformly doped well and a narrow undoped well, separated by a thin barrier. The optical absorption in that system is calculated, and the effects of the doping density are analysed as well as the effect the barrier thickness has on the absorption peaks. Finally the influence of an external electric field applied to the structure along the growth direction is examined. This work is organized as follows: Sect. 2 describes the model, Sect. 3 discusses the results of numerical simulations for the ADQW, and Sect. 4 concludes the paper with a brief closing summary.

2 Theoretical model

The one-dimensional Schrödinger equation which governs the wave functions of bound states reads:

$$-\frac{\hbar^2}{2}\frac{d}{dz}\frac{1}{m^*(z)}\frac{d\psi(z)}{dz}+V(z)\psi(z)=E\psi(z), \tag{1}$$

where $\psi(z)$ is the envelope wave function, E is the eigenvalue of energy, m^* is the effective mass, $V(z)$ is the total effective potential. The shooting method (Harrison and Valavanis 2016) is used to solve the Schrödinger equation for the potential $V(z)$ and acquire the energy eigenvalues E_k corresponding to the wave functions $\psi_k(z)$. The effective mass is here assumed to be constant within the heterostructure. In finite gap semiconductors non-parabolicity is characterized by energy and/or temperature dependent mass and is taken as a weak effect as it must be sufficiently close to the band edge with a finite gap (Chen et al. 2013; Vuković et al. 2014). The material system that we consider in this work has wide energy gap thus the band non-parabolicity can be neglected.

The one-dimensional Poisson's equation reads:

$$\frac{d^2\varphi(z)}{dz^2}=-\frac{\rho(z)}{\varepsilon(z)}, \tag{2}$$

where $\varphi(z)$ is the electrostatic potential, $\varepsilon(z)$ is the dielectric constant and $\rho(z)$ is the charge density. If assumed that the dopants are fully ionized, the charge density can be written as:

$$\rho(z)=q\left(N_d^+(z)-N_a^-(z)+p(z)-n(z)\right), \tag{3}$$

where q is the electron charge, N_d^+ is the density of ionized donors, N_a^- is the density of ionized acceptors, $p(z)$ is the density of holes and $n(z)$ is the density of electrons. By solving the Eq. (2) the value of $\varphi(z)$ is obtained, which is further used to generate the potential energy $V(z)$ as:

$$V(z)=-q\varphi(z)-qFz+\Delta E_c(z)+V_{xc}, \tag{4}$$

where ΔE_c represents the potential energy discontinuity due to the band offset at the heterointerface, F is the externally applied electric field and V_{xc} is the local exchange correlation potential expressed as (Liu 2022):

$$V_{xc}(z) = -\frac{q^4}{32\pi^2\hbar^2}\frac{m^*}{\epsilon^*}\left(\frac{9\pi}{4}\right)^{\frac{1}{3}}\frac{2}{\pi r_s^*}\left[1 + 0.054 r_s^* log\left(1 + \frac{11.4}{r_s^*}\right)\right]. \tag{5}$$

In the above expression the ϵ^* is the dielectric constant (assumed the same across the layers) and r_s^* is the parameter which represents an average distance between carriers scaled by the effective Bohr radius (Ando et al. 2003):

$$r_s^* = \sqrt[3]{\frac{3}{4\pi n(z)}}\frac{1}{a_B^*}, \tag{6}$$

where $a_B^* = \frac{4\pi\epsilon^*\hbar^2}{m^* q^2}$ is the effective Bohr radius. Potential energy calculated from Eq. (4) is then used in Eq. (1). Equations (1) and (2) are then solved self-consistently as in (Datta 2005; Gös 2011). After obtaining the electronic structure, the next step is the evaluation of the intersubband absorption between the relevant energy levels.

The probability for the electron in the initial state i, with the corresponding wave function Ψ_i and energy E_i, to transition to the final state f with a corresponding wave function Ψ_f and energy E_f ($E_f > E_i$) is given by (Harrison and Valavanis 2016):

$$W_{if} = \frac{2\pi}{\hbar}\left|H'_{if}\right|^2\delta\left(E_f - E_i - \hbar\omega\right), \tag{7}$$

where $\hbar\omega$ is the photon energy that has been absorbed. Both the initial and the final state belong to the same (conduction) band. Given that the absorption and the emission occur simultaneously in the structure, in order to calculate the effective absorption coefficient, the difference between these two processes must be observed within the entire subband, so Eq. (7) becomes (Vuković et al. 2022):

$$\begin{aligned} w_{if} = 2\sum_{k_x k_y}\frac{2\pi}{\hbar}\left|H'_{if}\right|^2\big(&f_{FD}\left(E_i\left(k_t^2\right), E_F\right)\left(1 - f_{FD}\left(E_f\left(k_t^2\right), E_F\right)\right) \\ &- f_{FD}\left(E_f\left(k_t^2\right), E_F\right)\left(1 - f_{FD}\left(E_i\left(k_t^2\right), E_F\right)\right)\big)\delta\left(E_f - E_i - \hbar\omega\right), \end{aligned} \tag{8}$$

where the first term in the sum represents the probability that the i-th state is filled and f-th state is unoccupied, while the second term represents the probability that the f-th state is occupied and i-th state is empty. Here $k_t = \sqrt{k_x^2 + k_y^2}$ corresponds to the transverse wave vector perpendicular to the growth direction of the layers.

The absorption coefficient of EM radiation passing through a structure is determined as:

$$\alpha_{if} = \frac{w_{if}\hbar\omega}{VI}, \tag{9}$$

where V is the volume of the structure, and I is the intensity of the EM radiation. By inserting Eq. (8) into Eq. (9) after summing up over the initial and the final subband, the final expression for fractional absorption reads (Harrison and Valavanis 2016):

$$A_{if} = \frac{q^2 \omega \pi}{\varepsilon_0 n_r c} \left| d_{if} \right|^2 L\left(\hbar\omega, \hbar\omega_0\right)\left(N_{si} - N_{sf}\right), \tag{10}$$

where $L\left(\hbar\omega, \hbar\omega_0\right)$ is the Lorenzian with the width equal to Γ, which is taken as 10% of the energy between relevant energy levels, n_r is the refractive index, c is the speed of light, N_{si} and N_{sf} are sheet carrier densities i.e. the number of electrons per unit of cross-section area for the initial and final subband respectively and d_{if} is the transition dipole matrix element.

3 Results and discussion

In this section the numerical results of the SP solver (Gös 2011; NEVOU 2022) for $ZnO/Zn_{0.7}Mg_{0.3}O$ ADQW structure are presented, where the quantum well (QW) material is ZnO. Quantum wells are $t_{qw1} = 2.5$ nm and $t_{qw2} = 1.5$ nm wide and the wider QW is uniformly dopped with Ga of concentration $N_d \simeq 5 \times 10^{19}\,\mathrm{cm}^{-3}$ as in (Meng et al. 2019) in order to populate the ground energy level. The effective mass in the well and barrier is taken as equal, and it reads $m^* = 0.28m_0$. The barrier material is $Zn_{0.7}Mg_{0.3}O$ alloy with varying thickness between $t_b = 0.5$ nm and $t_b = 1.5$ nm. Conduction band offset is calculated as $\Delta E_c = 0.675\Delta E_g$ which is ~ 506 meV as in (Meng et al. 2019).

Throughout the numerical simulations, the temperature is set to T = 300 K. Figure 1 shows the conduction band diagram of ADQW (a) without external electric field and (b) in external electric field F applied along the growth direction. The thickness of the barrier between the two wells is $t_b = 0.5$ nm, while the barriers surrounding the structure are 5 nm thick. Note that the ground and the second bound states are located within the wider well (t_{qw1}), while the first bound state is confined within the narrower well (t_{qw2}).

Notice in Fig. 2 that the A_{01} absorption peak decreases while the A_{02} peak increases with the rise in barrier thickness between the two QWs. Absorption peak A_{01} has the highest value of 6,8% for the smallest barrier length $t_b = 0.5$ nm. As the barrier becomes thicker, we see that besides the domination of A_{02} there is also its redshift by 30 meV, while the A_{01} peak position is almost unaffected. As the barrier thickness increases from 0.5 to 1.5 nm, the coupling between the two QWs decreases. Given that the envelope wavefunctions are confined in QWs, increasing the distance between the wells decreases the wavefunction overlap, thus decreasing the absorption peaks. The distance between the two peaks also depends on the energy differences E01 and E12 and that depend on the coupling between the QWs.

Figure 3 illustrates the changes in the absorption spectrum with different Ga concentrations in the wider well (the left well in Fig. 1). Note that with the increased well doping, the absorption peaks also increase, and the transition energy of A_{01} undergoes a blueshift.

The variation of the external electric field strength and its effect on the absorption spectra is also taken into account. The values of the applied electric field are varied from $F = +2.5 \times 10^7 \frac{V}{m}$ to $= -2.5 \times 10^7 \frac{V}{m}$. The results are shown in Fig. 4. The highest fractional absorption is achieved for $F = +2.5 \times 10^7 V/m$. Figure 1a, b demonstrate that the doping of the wider well bends the potential to the opposite side in comparison to the effect of the external field directed along the negative z-axis. The field thus compensates for the partial curvature and the peak A_{02} stays around 310 meV but gradually lowers from 2.3 to 1.9%. For the positive values of the external field, the peak A_{01} gradually blueshifts by 40 meV and lowers to 6%. We note that the peaks A_{01} and A_{12} add up as we increase the field. In

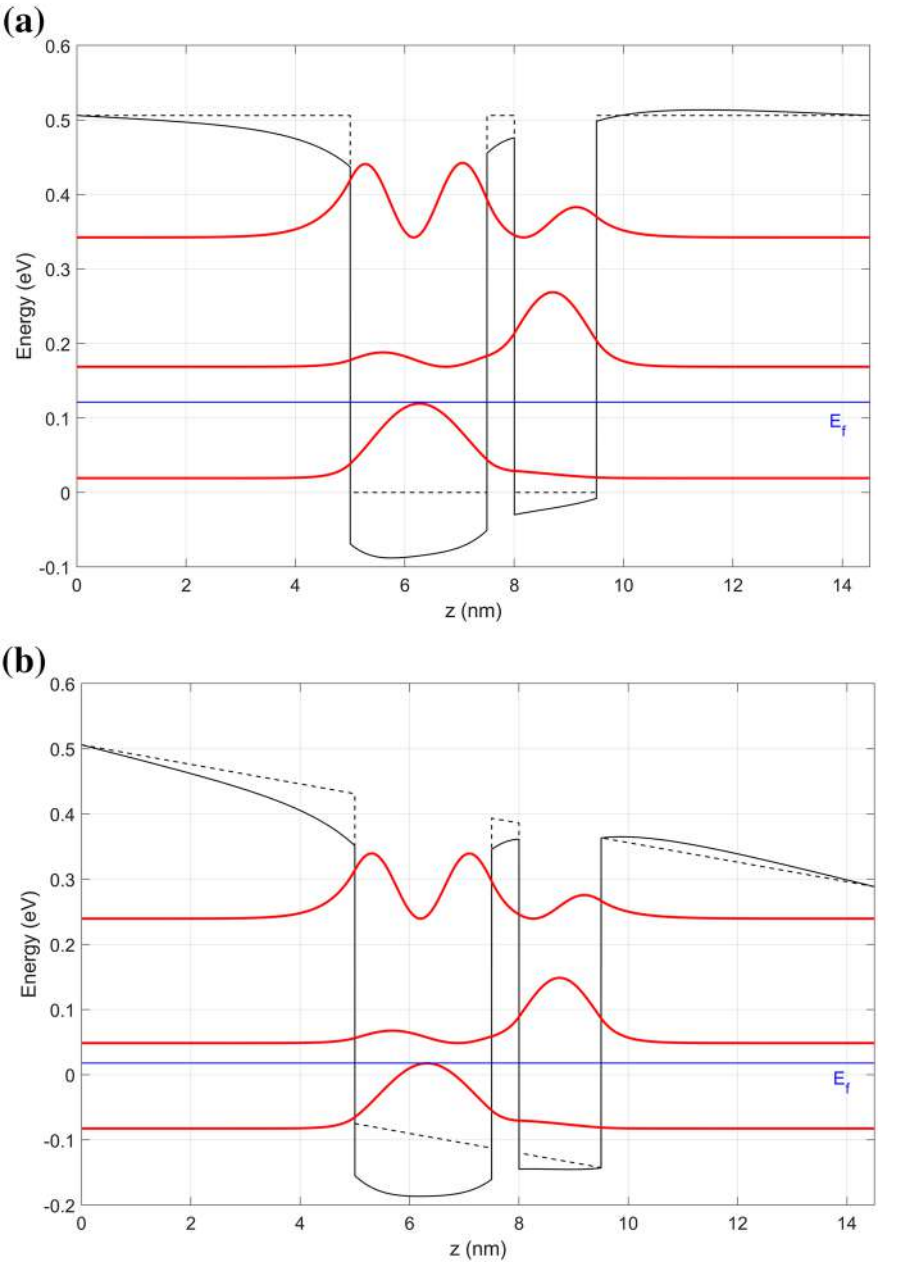

Fig. 1 Conduction-band diagram and the first three wavefunctions for $F=0$ (**a**) and $F = 1.5 \times 10^7 \frac{V}{m}$ (**b**). Bound states and their corresponding wave functions are denoted with full red lines. The potential without the effect of the wider well doping is demonstrated by the dashed black line. The bending of the potential due to doping is shown with a full black line. The Fermi level lies between the first and the second bound state denoted by a blue line

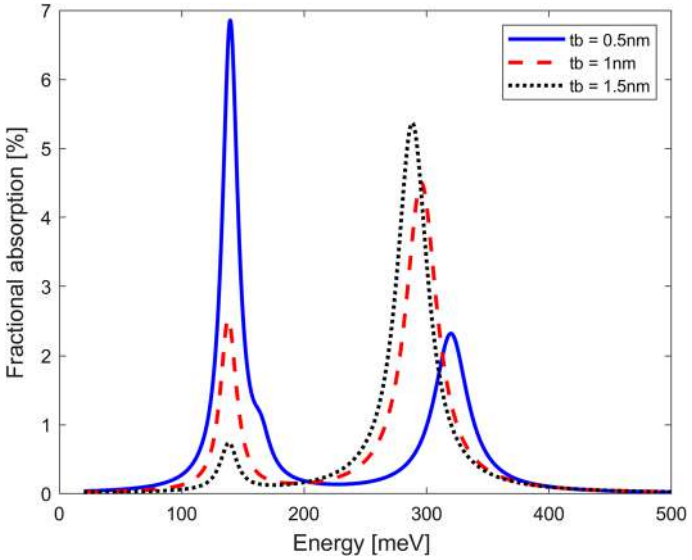

Fig. 2 Fractional absorption spectra for 3 different barrier thicknesses with the same doping density $N_d \simeq 5 \times 10^{19}$ cm^{-3}. From left to right the first major absorption peak corresponds to the transition between the ground and the first bound state (A_{01}). The second peak corresponds to the transitions between the ground and the second bound state (A_{02})

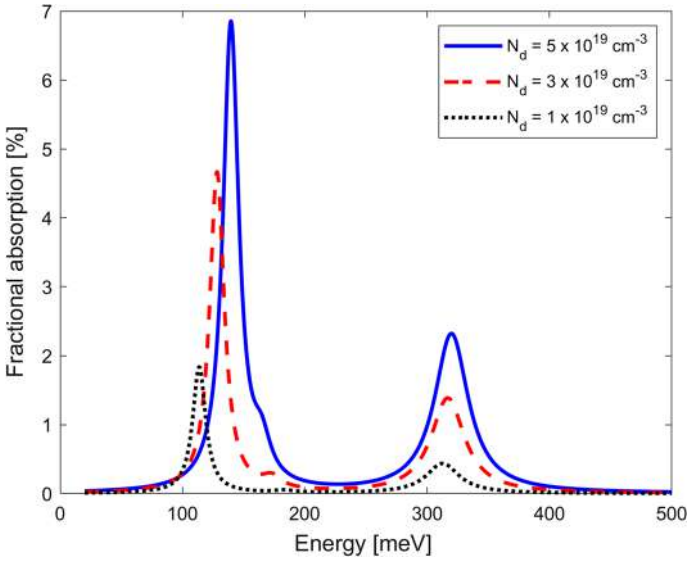

Fig. 3 Fractional absorption peaks for 3 different values of doping density N_d for the fixed barrier width $t_b = 0.5$ nm. The blue line is the same absorption spectrum as in Fig. 2, blue line

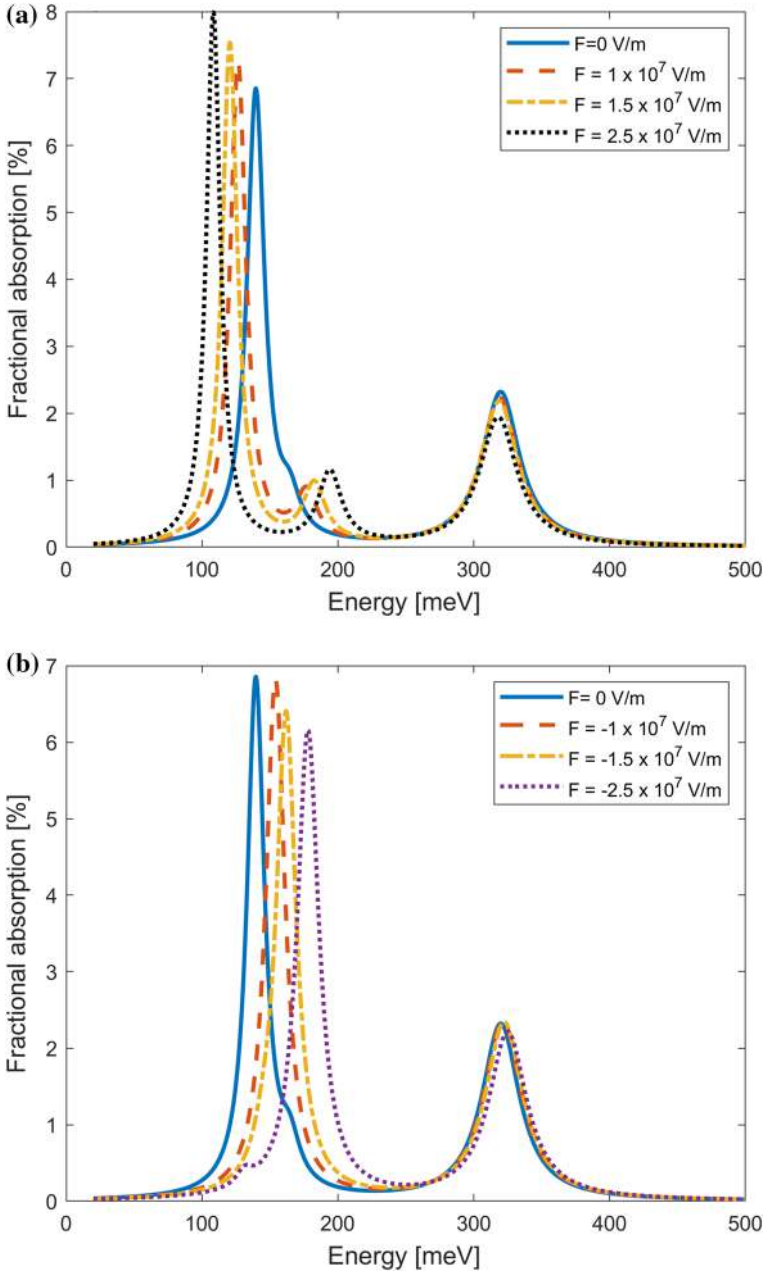

Fig. 4 Absorption spectra for different magnitudes of applied electric field for the fixed barrier width $t_b = 0.5$ nm and fixed doping density $N_d \simeq 5 \times 10^{19}$ cm^{-3}. The electric field is varied between $F = 0\frac{V}{m}$ and $F = 2.5 \times 10^7 \frac{V}{m}$ (**a**) and between $F = -2.5 \times 10^7 \frac{V}{m}$ and $F = 0\frac{V}{m}$ (**b**)

Fig. 4a let us focus on blue and yellow spectral lines that correspond to the same field strengths that are shown in Fig. 1a, b for energy band diagram and wave functions. One can see from Fig. 1 that the energy difference between the ground and first excited state E01 decreases with the applied electric field (+ sign), while the energy difference E02 is roughly the same in (a) and (b). This is reflected on Fig. 4a where the dominant absorption peak redshifts with applied electric field. Furthermore, externally applied electric field additionally bends the potential which slightly increases the confinement of wavefunctions or the wavefunction overlap (although not visible on Fig. 1) that results in change in the dominant absorption peak.

4 Summary

In this work we have numerically investigated fractional absorption for ADQW structure. We have solved self-consistently the SP system for a promising new semiconductor material, obtained the electron eigen energies, wave functions and carrier distributions, and calculated fractional absorption for the intersubband transitions. Absorption spectra for different barrier thicknesses, doping concentrations and different magnitudes of an external electric field have been considered. The barrier thickness is shown to change which absorption peak is dominant, while the doping densities affect the maxima of the absorption in the same direction. As demonstrated, fractional absorption can also be modified by applying an external electric field. Our future work will be directed towards considering more complex QW structures, with the final goal of optimizing an active region of a quantum cascade laser.

Author contributions All authors contributed to the study conception and design. Material preparation, data collection and analysis were performed by all authors. The first draft of the manuscript was written by Aleksandar Atić and all the authors contributed in finalizing the previous versions of the manuscript. All authors have read and approved the submitted version of the manuscript.

Funding This work was supported by Ministry of Education, Science and Technological Development (Republic of Serbia): Grant Number 450-03-68/2022-14/200017; "Multi-Scale Modelling of Terahertz Quantum Cascade Laser Active Regions", Multilateral scientific and technological cooperation in the Danube region 2020–2021 (Grant Number 337–00–00322/2019–09/221); and "DEMETRA: Development of high-performance mid-IR/THz quantum cascade lasers for advanced applications", Science Fund of the Republic of Serbia, Serbian Science and Diaspora Collaboration Programme: Knowledge Exchange Vouchers (Grant Number 6436915).

Data availability Not applicable.

Declarations

Ethical approval Not applicable.

Competing interests The authors have no relevant financial or non-financial interests to disclose.

References

Ando, T., Taniyama, H., Ohtani, N., Nakayama, M., Hosoda, M.: Self-consistent calculation of subband occupation and electron–hole plasma effects: variational approach to quantum well states with Hartree and exchange-correlation interactions. J. Appl. Phys. **94**, 4489–4501 (2003). https://doi.org/10.1063/1.1606512

Bellotti, E., Paiella, R.: Numerical simulation of ZnO-based terahertz quantum cascade lasers. J. Electron. Mater. **39**, 1097–1103 (2010). https://doi.org/10.1007/s11664-010-1206-4

Cao, X., Wang, H., Hu, M., Jia, Z.: Exciton states in ZnO/MgZnO quantum wells under electric field and magnetic field. Phys. Solid State. **63**, 1137–1144 (2021). https://doi.org/10.1134/S1063783421080059

Chen, S., Zhan, T., Pan, X., He, H., Huang, J., Lu, B., Ye, Z.: UV electroluminescence emissions from high-quality ZnO/ZnMgO multiple quantum well active layer light-emitting diodes. RSC Adv **11**, 38949–38955 (2021). https://doi.org/10.1039/d1ra06685d

Chen, X., Parker, D., Singh, D.J.: Importance of non-parabolic band effects in the thermoelectric properties of semiconductors. Sci. Rep. **3**, 3168 (2013). https://doi.org/10.1038/srep03168

Dakhlaoui, H., Nefzi, M.: Enhancement of the optical absorption in MgZnO/ZnO quantum well under external electric field. Optik (stuttg) **157**, 1342–1349 (2018). https://doi.org/10.1016/j.ijleo.2017.12.107

Datta, S.: Quantum Transport: Atom to Transistor. Cambridge University Press, Cambridge (2005)

Dubajić, M., Daničić, A., Vuković, N., Milanović, V., Radovanović, J.: Optimization of cubic GaN/AlGaN quantum cascade structures for negative refraction in the THz spectral range. Opt. Quantum Electron. **50**, 373 (2018). https://doi.org/10.1007/s11082-018-1639-1

Faist, J.: Quantum Cascade Lasers. OUP, Oxford (2013)

Fujita, M., Suzuki, R., Sasajima, M., Kosaka, T., Deesirapipat, Y., Horikoshi, Y.: Molecular beam epitaxial growth of ZnMgO/ZnO/ZnMgO single quantum well structure on Si(111) substrate. J. Vac. Sci. Technol. B Microelectron. Nanom. Struct. **24**, 1668–1670 (2006). https://doi.org/10.1116/1.2200381

Gajić, A., Radovanović, J., Vuković, N., Milanović, V., Boiko, D.L.: Theoretical approach to quantum cascade micro-laser broadband multimode emission in strong magnetic fields. Phys. Lett. A **387**, 127007 (2021). https://doi.org/10.1016/j.physleta.2020.127007

Gmachl, C., Ng, H.M., Cho, A.Y.: Intersubband absorption in GaN/AlGaN multiple quantum wells in the wavelength range of λ~1.75–4.2 μm. Appl. Phys. Lett. **77**, 334–336 (2000a). https://doi.org/10.1063/1.126968

Gmachl, C., Ng, H.M., George Chu, S.-N., Cho, A.Y.: Intersubband absorption at λ~1.55 μm in well- and modulation-doped GaN/AlGaN multiple quantum wells with superlattice barriers. Appl. Phys. Lett. **77**, 3722–3724 (2000b). https://doi.org/10.1063/1.1332108

Gös, W.: Hole trapping and the negative bias temperature instability. (2011) https://doi.org/10.34726/hss.2011.25057

Gruber, T., Kirchner, C., Kling, R., Reuss, F., Waag, A.: ZnMgO epilayers and ZnO-ZnMgO quantum wells for optoelectronic applications in the blue and UV spectral region. Appl. Phys. Lett. **84**, 5359–5361 (2004). https://doi.org/10.1063/1.1767273

Harrison, P., Valavanis, A.: Quantum Wells. Wires and Dots. Wiley, Chichester (2016)

He, J., Wang, P., Chen, H., Guo, X., Guo, L., Yang, Y.: Study on temperature effect on properties of ZnO/MgZnO based quantum cascade detector in mid-infrared region. Appl. Phys. Express **10**, 011101 (2017). https://doi.org/10.7567/APEX.10.011101

Higashiwaki, M., Kaplar, R., Pernot, J., Zhao, H.: Ultrawide bandgap semiconductors. Appl. Phys. Lett. **118**, 200401 (2021). https://doi.org/10.1063/5.0055292

Isić, G., Radovanović, J., Milanović, V.: Anisotropic spin-dependent electron tunneling in a triple-barrier resonant tunneling diode. J. Appl. Phys. **102**, 123704 (2007). https://doi.org/10.1063/1.2825401

Jirauschek, C., Kubis, T.: Modeling techniques for quantum cascade lasers. Appl. Phys. Rev. **1**, 011307 (2014). https://doi.org/10.1063/1.4863665

Kaminska, A., Duzynska, A., Nowakowska, M., Suchocki, A., Wassner, T.A., Laumer, B., Eickhoff, M.: Luminescent properties of ZnO and ZnMgO epitaxial layers under high hydrostatic pressure. J. Alloys Compd. **672**, 125–130 (2016). https://doi.org/10.1016/j.jallcom.2016.02.128

Köhler, R., Tredicucci, A., Beltram, F., Beere, H.E., Linfield, E.H., Davies, A.G., Ritchie, D.A., Iotti, R.C., Rossi, F.: Terahertz semiconductor-heterostructure laser. Nature **417**, 156–159 (2002). https://doi.org/10.1038/417156a

Lee, M., Wanke, M.C.: Searching for a solid-state terahertz technology. Science **316**, 64–65 (2007)

Li, S.M., Kwon, B.J., Kwack, H.S., Jin, L.H., Cho, Y.H., Park, Y.S., Han, M.S., Park, Y.S.: Optical transition dynamics in ZnO/ZnMgO multiple quantum well structures with different well widths grown on ZnO substrates. J. Appl. Phys. **107**, 033513 (2010). https://doi.org/10.1063/1.3284959

Liu, D.: Intersubband optical absorption in ZnO/MgZnO triple quantum well structures. Appl. Phys. B **128**, 74 (2022). https://doi.org/10.1007/s00340-022-07799-7

Liu, J., Zhou, Y., Zhai, S., Liu, F., Liu, S., Zhang, J., Zhuo, N., Wang, L., Wang, Z.: High-frequency very long wave infrared quantum cascade detectors. Semicond. Sci. Technol. **33**, 125016 (2018). https://doi.org/10.1088/1361-6641/aaebd4

Mang, A., Reimann, K., Rübenacke, S.: Band gaps, crystal-field splitting, spin-orbit coupling, and exciton binding energies in ZnO under hydrostatic pressure. Solid State Commun. **94**, 251–254 (1995). https://doi.org/10.1016/0038-1098(95)00054-2

Meng, B., Tamayo-Arriola, J., Le Biavan, N., Montes Bajo, M., Torres-Pardo, A., Hugues, M., Lefebvre, D., Hierro, A., Chauveau, J.M., Faist, J.: Observation of intersubband absorption in ZnO coupled quantum wells. Phys. Rev. Appl. **12**, 054007 (2019). https://doi.org/10.1103/PhysRevApplied.12.054007

NEVOU, L.: Q_SchrodingerPoisson1D_CB. https://github.com/LaurentNevou/Q_SchrodingerPoisson1D_CB

Ohtani, K., Belmoubarik, M., Ohno, H.: Intersubband optical transitions in ZnO-based quantum wells grown by plasma-assisted molecular beam epitaxy. J. Cryst. Growth. **311**, 2176–2178 (2009). https://doi.org/10.1016/j.jcrysgro.2008.09.134

Park, S.H., Ahn, D.: Spontaneous and piezoelectric polarization effects in wurtzite ZnO/MgZnO quantum well lasers. Appl. Phys. Lett. **87**, 1–3 (2005). https://doi.org/10.1063/1.2149294

Radosavljević, A., Radovanović, J., Milanović, V.: Optimization of cubic GaN/AlGaN quantum well-based structures for intersubband absorption in the infrared spectral range. Solid State Commun. **182**, 38–42 (2014). https://doi.org/10.1016/j.ssc.2013.12.006

Radosavljević, A., Radovanović, J., Milanović, V., Indjin, D.: Cubic GaN/AlGaN based quantum wells optimized for applications to tunable mid-infrared photodetectors. Opt. Quantum Electron. **47**, 865–872 (2015). https://doi.org/10.1007/s11082-014-0016-y

Radovanović, J., Milanović, V., Ikonić, Z., Indjin, D.: Optimization of spin-filtering properties in diluted magnetic semiconductor heterostructures. J. Appl. Phys. **99**, 073905 (2006). https://doi.org/10.1063/1.2188052

Radovanović, J., Milanović, V., Ikonić, Z., Indjin, D.: Application of the genetic algorithm to the optimized design of semimagnetic semiconductor-based spin-filters. J. Phys. D Appl. Phys. **40**, 5066–5070 (2007). https://doi.org/10.1088/0022-3727/40/17/010

Radovanovic, J., Milanovic, V., Ikonic, Z., Indjin, D., Jovanovic, V., Harrison, P.: Optimal design of GaN-AlGaN Bragg-confined structures for intersubband absorption in the near-infrared spectral range. IEEE J. Quantum Electron. **39**, 1297–1304 (2003). https://doi.org/10.1109/JQE.2003.817584

Radovanović, J., Vuković, N., Milanović, V.: Global Optimization methods for the design of MIR-THz QCLs applied to explosives detection. In: NATO Science for Peace and Security Series B: Physics and Biophysics. pp. 71–86 (2021)

Riane, H., Mokaddem, A., Temimi, L., Doumi, B., Bahlouli, S., Hamdache, F.: ZnO/ZnMgO: cubic quantum well laser in UV spectrum. Int. J. Adv. Manuf. Technol. **89**, 629–633 (2017). https://doi.org/10.1007/s00170-016-9105-3

Shirazi-HD, M., Turkmeneli, K., Liu, S., Dai, S., Edmunds, C., Shao, J., Gardner, G., Zakharov, D.N., Manfra, M.J., Malis, O.: Dramatic enhancement of near-infrared intersubband absorption in c-plane AlInN/GaN superlattices. Appl. Phys. Lett. **108**, 121108 (2016). https://doi.org/10.1063/1.4944847

Sirkeli, V.P., Hartnagel, H.L.: ZnO-based terahertz quantum cascade lasers. Opto-Electron. Rev. **27**, 119–122 (2019). https://doi.org/10.1016/j.opelre.2019.04.002

Solovyev, V.V., Kukushkin, I.V.: Two-subband occupation by 2D electrons in MgZnO/ZnO heterostructures. Appl. Phys. Express. **12**, 021001 (2019). https://doi.org/10.7567/1882-0786/aaf786

Solovyev, V.V., Van'kov, A.B., Kukushkin, I.V., Falson, J., Zhang, D., Maryenko, D., Kozuka, Y., Tsukazaki, A., Smet, J.H., Kawasaki, M.: Optical probing of MgZnO/ZnO heterointerface confinement potential energy levels. Appl. Phys. Lett. **106**, 082102 (2015). https://doi.org/10.1063/1.4913313

Sun, J.W., Zhang, B.P.: Well-width dependence of exciton–longitudinal-optical-phonon coupling in MgZnO/ZnO single quantum wells. Nanotechnology **19**, 485401 (2008). https://doi.org/10.1088/0957-4484/19/48/485401

Suzuki, N., Iizuka, N.: Feasibility study on ultrafast nonlinear optical properties of 1.55-μm intersubband transition in AlGaN/GaN quantum wells. Jpn. J. Appl. Phys. **36**, 1006–1008 (1997). https://doi.org/10.1143/JJAP.36.L1006

Tkach, N.V., Seti, J.A., Grynyshyn, Y.B.: Electron-phonon interaction in three-barrier nanosystems as active elements of quantum cascade detectors. Semiconductors **49**, 529–539 (2015). https://doi.org/10.1134/S1063782615040259

Vuković, N., Milanović, V., Radovanović, J.: Influence of nonparabolicity on electronic structure of quantum cascade laser. Phys. Lett. A **378**, 2222–2225 (2014). https://doi.org/10.1016/j.physleta.2014.04.069

Vukovic, N., Radovanovic, J., Milanovic, V.: Enhanced modeling of band nonparabolicity with application to a mid-IR quantum cascade laser structure. Phys. Scr. **T162**, 014014 (2014). https://doi.org/10.1088/0031-8949/2014/T162/014014

Vuković, N., Radovanović, J., Milanović, V.: Refined modelling of anisotropy influence on the optical gain in Mid-IR quantum cascade lasers. Opt. Quantum Electron. **54**, 380 (2022). https://doi.org/10.1007/s11082-022-03742-4

Vukovic, N., Radovanovic, J., Milanovic, V., Boiko, D.L.: Analytical expression for Risken–Nummedal–Graham–Haken instability threshold in quantum cascade lasers. Opt. Express **24**, 26911 (2016a). https://doi.org/10.1364/OE.24.026911

Vukovic, N., Radovanovic, J., Milanovic, V., Boiko, D.L.: Multimode RNGH instabilities of Fabry–Pérot cavity QCLs: impact of diffusion. Opt. Quantum Electron. **48**, 254 (2016b). https://doi.org/10.1007/s11082-016-0515-0

Vukovic, N., Radovanovic, J., Milanovic, V., Boiko, D.L.: Numerical study of Risken–Nummedal–Graham–Haken instability in mid-infrared Fabry-Pérot quantum cascade lasers. Opt. Quantum Electron. **52**, 91 (2020). https://doi.org/10.1007/s11082-020-2210-4

Vukovic, N.N., Radovanovic, J., Milanovic, V., Boiko, D.L.: Low-threshold RNGH instabilities in quantum cascade lasers. IEEE J. Sel. Top. Quantum Electron. **23**, 1–16 (2017). https://doi.org/10.1109/JSTQE.2017.2699139

Zhang, B.P., Liu, B.L., Yu, J.Z., Wang, Q.M., Liu, C.Y., Liu, Y.C., Segawa, Y.: Photoluminescence and built-in electric field in ZnO/$Mg_{0.1}Zn_{0.9}O$ quantum wells. Appl. Phys. Lett. **90**, 132113 (2007). https://doi.org/10.1063/1.2716367

Zhao, K., Chen, G., Li, B.-S., Shen, A.: Mid-infrared intersubband absorptions in ZnO/ZnMgO multiple quantum wells. Appl. Phys. Lett. **104**, 212104 (2014). https://doi.org/10.1063/1.4880816

Zhu, J., Ban, S.L., Ha, S.H.: A simulation of intersubband absorption in ZnO/$Mg_xZn_{1-x}O$ quantum wells with an external electric field. Superlattices Microstruct. **56**, 92–98 (2013). https://doi.org/10.1016/j.spmi.2012.11.011

Zhu, J., Kuznetsov, A.Y., Han, M.S., Park, Y.S., Ahn, H.K., Ju, J.W., Lee, I.H.: Structural and optical properties of ZnO$Mg_{0.1}Zn_{0.9}O$ multiple quantum wells grown on ZnO substrates. Appl. Phys. Lett. **90**, 211909 (2007). https://doi.org/10.1063/1.2742574